2007 International Nuclear Atlantic Conference - INAC 2007
Santos, SP, Brazil, September 30 to October 5, 2007
ASSOCIAÇÃO BRASILEIRA DE ENERGIA NUCLEAR - ABEN
ISBN: 978-85-99141-02-1

Aramis: A COMPUTER CODE TO ESTIMATE TOTAL AND PEAK EFFICIENCIES OF AN HPGe PHOTON DETECTOR

Luzia Venturini[1], Nora L. Maidana[2] and Vito R. Vanin[2]

[1] Instituto de Pesquisas Energéticas e Nucleares (IPEN / CNEN - SP)
Av. Professor Lineu Prestes 2242
05508-000 São Paulo, SP
lventur@ipen.br

[2] Universidade de São Paulo – Departamento de Física Experimental
Rua do Matão, Travessa R, 187
05315-970 São Paulo, SP
nmaidana@if.usp.br
vanin@if.usp.br

ABSTRACT

In this work, the total and peak efficiencies of a coaxial HPGe photon detector were evaluated by Monte Carlo simulation, and the accuracy of the simulated results was tested experimentally. The photon interaction with the detector was taken into account in detail. A geometric model of the detector was employed, including, besides the detector crystal active volume, the electric contacts, an empty internal region and dead layers at the crystal surface and contact regions. The dimensions of these regions and crystal length and radius were adjusted in order to fit the experimental efficiencies for the gamma-rays from a ^{166m}Ho point source, resulting in values somewhat, but meaningfully, different from those stated on the detector's operation manual. The measurements were taken with the source placed far from the detector in order to minimize summing losses. The code was used to predict total and peak efficiencies for the gamma rays of ^{65}Zn and ^{54}Mn activity-calibrated sources. The simulated results were in agreement with experimental data. Simulations with the MCNP code, using the same detector model, give very similar peak efficiencies and somewhat different total efficiencies. The method allows accurate prediction of the experimental efficiencies.

1. INTRODUCTION

The calculation of peak and total efficiencies of an HPGe detector from its physical properties should take the different types of interaction of radiation with matter and detector dimensions and characteristics into account. Some details of the HPGe crystal and capsule, however, are usually not described in the detector operation manual, requiring to their determination the analysis of spectra taken with gamma radiation of specially selected energies, in such a way that the gamma-rays mean free paths are distributed conveniently inside the detector active volume. By measuring the experimental efficiency for these gamma-rays, preferably using few radionuclides, it is possible to adjust the dimensions of a geometric model representing the detector.

In this approach, the detector behavior can be reproduced without detailed knowledge of its internal structure. Once the model parameters are determined from the fit of the experimental values obtained with the selected sources, the efficiency can be predicted for any gamma-ray energy from sources placed anywhere, making easier to deal with extended sources whose shapes or densities are unsuitable for calibration standards preparation.

The efficiency calculations can be done using the Monte Carlo Method [1], by random sorting the interaction processes of radiation with matter, and computing the amount of energy deposited in each interaction. Only those photons that deposit all their initial energy inside the detector active volume are counted to determine the peak efficiency, while for the total efficiency all photons that deposit at least a fraction of their initial energy are counted.

The detector dimensions were chosen as the values that minimize the difference between experimental and calculated peak efficiencies measured for sources placed sufficiently far from the detector to avoid the contribution of sum effects. The peak and total efficiencies were simulated considering the four main types of interaction of the radiation in the energy range used: photoelectric and Compton effects, coherent scattering and pair production. The object-oriented computer program was written in C++.

2. MATERIALS AND METHODS

2.1. Detector Model

We used a 162 cm^3 active volume HPGe detector, type P, produced by EG&G Ortec; the dimensions quoted in the factory data sheet are given in Table 1. In the simulation, the detector is represented by a cylindrical crystal whose active volume is delimited by dead layers along its external surface and around the central cavity, partially filled by a aluminum contact, and is installed inside an aluminum capsule, as shown in Fig.1. All other dimensions needed to simulate the detection process, particularly those related to the inner contact, are not given by the manufacturer and were deduced from spectra taken with point sources of ^{241}Am (3286 ± 0.33%) Bq, ^{166m}Ho (3017 ± 1.6 %) Bq, and ^{60}Co (1019.6 ± 0.11 %) Bq. To achieve good fitting, however, it was needed to change some of the dimensions given in the manual, particularly the dead layer thickness, as will be shown in section 3.

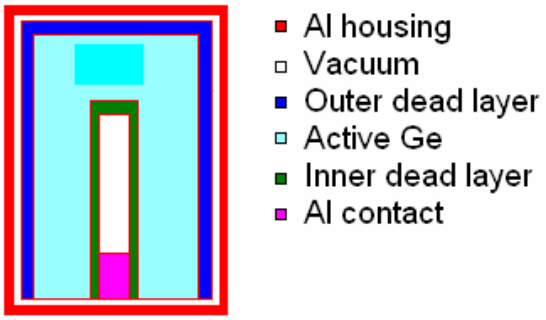

Figure 1. Cross-section of the detector, along the symmetry axis, in the geometric representation.

2.2. Monte Carlo Method [1]

In sections 2.3 to 2.7, we will show the algorithms used in the developed computer program, named **Aramis,** for sorting interaction type, path length, scattering angle, and energy of photons and electrons along the history created by each primary photon in the detector. We will represent by *r* a random number uniformly distributed between 0 and 1, obtained with a random number generator with long period ($>10^9$) [2].

The number of histories *m* required to reach a given relative uncertainty δ in the efficiency can be estimated assuming that the number of histories *n* that are assigned as detection events are distributed according a binomial probability function, with probability $p = \frac{n}{m}$. Since both *n* and *m* are big numbers, the probability function of the quantity

$$t = \delta \sqrt{\frac{m.p}{(1-p)}} \tag{1}$$

is approximately normal with variance one; hence, once chosen the desired relative uncertainty at a given confidence level, the number of histories required can be found.

2.3. Photon trajetory

In a uniform medium with linear attenuation coefficient μ, the photon free path *L* is randomly sorted by:

$$L_r = \frac{-\ln(r)}{\mu} \tag{2}$$

For point sources, photons are always emitted from the same position, in random directions (α,β,γ) sorted according to:

$$\cos \gamma = 2\, r_1 - 1 \tag{3}$$

$$\delta = \pi\, (2\, r_2 - 1) \tag{4}$$

$$\cos \alpha = \sin \gamma \cos \delta \tag{5}$$

$$\cos \beta = \sin \gamma \sin \delta, \tag{6}$$

where r_1 e r_2 are random numbers between 0 and 1.

2.4. Inelastic Scattering

The Compton scattering angular distribution of a photon with energy *E* was assumed to be given by the Klein-Nishina equation [1]:

$$\frac{d\sigma_E(\Omega)}{d\Omega} = \frac{r_o^2}{2}\frac{1+\cos^2\theta}{\left[1+E(1-\cos\theta)\right]^2}\left\{1+\frac{E^2(1-\cos\theta)^2}{(1+\cos^2\theta)\left[1+E(1-\cos\theta)\right]}\right\} \tag{7}$$

The energy of the scattered photon, E^*, is

$$E^* = \frac{E}{1+E(1-\cos\theta)} \tag{8}$$

where θ is the photon scattering angle, and both E and E^* are in $m_e c^2$ units. Using:

$$d\sigma_E(E^*) = d\sigma_E(\Omega)d\Omega = -\sigma_E(\Omega)\cdot 2\pi \cdot d(\cos\theta) \tag{9}$$

$$v = 1+\frac{1}{E}-\frac{1}{E^*} \tag{10}$$

$$w = \frac{E}{1+2E} \tag{11}$$

$$r = \left[\int_w^v \sigma_E(E^*)dE^*\right].\left[\int_w^E \sigma_E(E^*)dE^*\right]^{-1} \tag{12}$$

$$g(v) = \int \sigma_E(E^*)dE^* = \frac{1}{2E}v^2 + \frac{2E+1}{E^2}v + \frac{E^2-2E-2}{E}\ln(v) - \frac{1}{v} \tag{13}$$

we arrive at:

$$r\cdot\left[g(E)-g(w)\right] = g(v)-g(w) \tag{14}$$

Equation (14) allows us to find v for a given random r. The solutions of this equation were achieved numerically by an interactive method [3].

The direction of the initial electron motion is known once the photon scattering angle is determined. The cosine of the electron scattering angle is given by:

$$\cos\varphi = \frac{E-E^*\cos\theta}{\sqrt{(E-E^*)^2+2.(E-E^*)}}\,. \tag{15}$$

2.5. Photoelectric Effect

In this process, the photon interacts with a bounded electron, which is ejected with kinetic energy corresponding to the difference between the photon energy and the electron binding

energy. The angular distribution of an electron emitted with kinetic energy E_e was assumed to be described by [4]:

$$\frac{d\sigma}{d(\Omega)} \approx \frac{\sin^2\theta}{(1-\beta\cos\theta)^4}\left\{1+\frac{1}{2}\gamma\cdot(\gamma-1))(\gamma-2)\cdot(1-\beta\cos\theta)\right\} \tag{16}$$

where:

$$\gamma = 1+\frac{E_e}{m_e c^2} \tag{17}$$

$$\beta = \frac{\sqrt{E_e(E_e+2m_e c^2)}}{E_e+m_e c^2} \tag{18}$$

and θ is the electron scattering angle. Using:

$$u = 1-\beta\cos\theta \tag{19}$$

$$b = \frac{1}{2}\gamma\cdot(\gamma-1)(\gamma-2) \tag{20}$$

$$g(u) = -\int d\sigma\cdot sen\theta\cdot d\theta = \frac{\beta^2-1}{3u^3}+\frac{(\beta^2-1)\cdot b-2}{2u^2}+\frac{1-2b}{u}+b\ln(u) \tag{21}$$

we find:

$$r\cdot[g(1-\beta)-g(1+\beta)] = g(u)-g(1+\beta) \tag{22}$$

Eq. (22) allows us to sort cos θ directly from a given random number r uniformly distributed. The solutions of Eq. (22) were achieved using the same interactive method used to solve equation (14) [3].

2.6. Coherent Scattering

In coherent scattering, photons do not lose energy. The angular distribution was obtained in tabular format from the calculations of Lynn Kissel [5], in the modified form factor with angle independent anomalous scattering factors approximation. The scattering angles and their respective probabilities were numerically integrated and normalized to give an angular probability distribution between 0 and 1. The table was used to interpolate the scattering angles for a given energy and a random *r.*

2.7. Pair Production

We considered that the photon converts its energy in rest mass and kinetic energy of an electron-positron pair, which will move in the crystal in random directions. The kinetic

energy is also shared between electron and positron with uniform random distribution, and one of the particles, chosen randomly, is selected to be the positron, which will be transported like an electron; in consequence, the tables of range of electrons are used to determine whether or not it escapes from the active volume.

When the positron does not escape from the crystal, it creates two annihilation photons that are emitted in opposite directions, with an isotropic angular distribution. Each of the annihilation photons either interacts inside the active volume and deposit all or part of its energy in the detector active volume or escape from the crystal; the same procedure described in the previous sections is applied to compute the deposited energy. The histories where the annihilation photon interacts inside the active volume but the ejected electron stops outside, were accounted for the total efficiency and not for the peak efficiency; the same was done when the photon interacts in the dead layer but the electron stops in the detector active volume.

3. RESULTS

Table 1 shows the adjusted dimensions of the various regions in the detector model compared to the nominal values from the detector's operation manual. The values were adjusted until the simulated peak efficiencies coincided with the experimental values obtained in the measurement of the point sources. Other authors [6,7] have already pointed out differences between the nominal dimensions of their detectors and the values that they obtained in similar studies.

Table 1. Detector nominal and adjusted dimensions.

Parameter	Nominal (cm)	Adjusted (cm)
Crystal height	5.9	5.9
Crystal radius	2.95	2.95
Diameter of the Al contact	-	0.47
Length of the Al contact	-	0.50
Diameter of the empty cylinder	-	0.47
Length of the empty cylinder	-	4.0
Thickness of the lateral outer dead layer	0.070	0.160
Thickness of the lateral inner dead layer	-	0.170
Thickness of the frontal outer dead layer	-	0.130
Thickness of the frontal inner dead layer	-	0.160
Thickness of the Al housing	0.127	0.127
Distance from crystal to Al housing	0.3	0.3

Table 2 shows the energies (E), the experimental (ε_E) and simulated (ε_P) peak efficiencies, and the simulated total efficiencies (ε_T). The experimental results correspond to the interpolated values from the fit of a non-linear function [8] to the raw data, in order to reduce the statistical fluctuation**.** The partial cross sections for each interaction type and the electron range tables used in the simulation were taken from the MCNP data [9]. The relative uncertainty in the simulated efficiencies is $\delta = 1.4$ % at the 97% confidence level. Energies and gamma intensities were taken from LNHB/CEA [10,11,12,13,14].

Table 2. Experimental and simulated efficiencies used in the fitting procedure of the dimensions of the detector.

Radionuclide	E (keV)	$\varepsilon_P\ 10^{-3}$	$\varepsilon_T\ 10^{-3}$	$\varepsilon_E\ 10^{-3}$
^{241}Am	59.549	1.125	1.177	1.123 (15)
^{166}Ho	80.57	2.391	2.550	2.37 (5)
	184.41	3.027	3.993	3.02 (5)
	280.46	2.241	3.937	2.31 (2)
	410.94	1.609	3.792	1.603 (12)
	529.80	1.284	3.677	1.304 (9)
	711.68	1.006	3.524	1.023 (6)
	778.82	0.934	3.478	0.949 (5)
	810.28	0.921	3.461	0.918 (5)
	950.97	0.806	3.363	0.803 (5)
^{60}Co	1173.24	0.689	3.231	0.682 (10)
	1332.50	0.622	3.151	0.619 (9)

4. DISCUSSION

4.1. Summary of the Simulated Histories

Table 3 summarizes the statistics of the events that occurs in the detector, for some gamma-ray energies. For each count in the full energy absorption peak there is just one photoelectric event, except for energies above 1.02 MeV, when two events can happen since two annihilation gammas rays can be produced and must be completely absorbed inside the crystal to contribute to the peak efficiency. In this case, the average photoelectric events may be greater than 1.0, as can be seen for the 1332 keV gamma ray.

It is expected that the average number of interactions for the gamma rays which contribute to the peak efficiency is near 1.0 at low energies, which can be observed from the data shown in Table 3, being 1.22 at 59 keV. This value increases as the photon energy increases, as expected from the decrease in photoelectric cross-section accompanied by the increase in

Compton scattering cross-section, attaining 4.0 interactions before complete absorption at 1332 keV.

Table 3. Peak and total detection event-type statistics obtained in the simulation, for some gamma-ray energies.

	59.54 keV	80.57 keV	280.46 keV	410.94 keV	711.68 keV	1332.5 keV
Million of histories	45	22	28	32	51	82
Random numbers (10^6)	92	43	47	65	104	168
Peak						
Coherent events/count	0.16145	0.153	0.165	0.153	0.145	0.1429
Compton events/count	0.06169	0.143	1.495	1.985	2.502	2.8423
Photoelectric events/count	1.0	1.0	1.0	1.0	1.0	1.0006
Pair events/count	-	-	-	-	-	0.0006
Average number of interactions	1.223	1.296	2.66	3.138	3.647	3.9864
Peak counts	51143	51078	51086	51118	51149	51169
Total						
Coherent events/count	0.16138	0.155	0.178	0.151	0.108	0.0792
Compton events/count	0.09747	0.199	1.621	1.927	2.079	2.0554
Photoelectric events/count	0.99968	0.996	0.696	0.541	0.379	0.2731
Pair events/count	-	-	-	-	-	0.0038
Average number of interactions	1.2585	1.35	2.495	2.619	2.566	2.4115
Total number of counts	53527	54486	89747	120473	179150	259221

In what relates to the total efficiency, the average number of interactions increases from 1.26 interactions at 59 keV to 2.5 at 280 keV, and then decreases slowly with increasing energy, which can be related to the increase in average energy of Compton scattered photons, when they are more likely to escape from the active detector volume.

Fig. 2 shows the angular distribution of scattered photons and electrons inside the detector, resulting from multiple interactions, for incident photons with initial energies 80, 711 and 1332 keV. The photon energy changes during the attenuation process and the energy variation will increase with the photon initial energy.

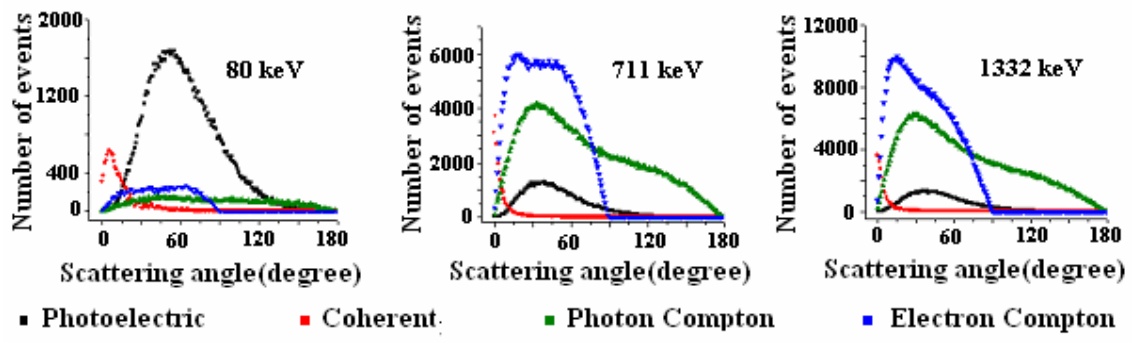

Figure 2. Angular distributions of gamma-rays and electrons scattered inside the detector for 80, 711 and 1332 keV incident photons.

4.2. Comparison with Independent Experimental Data

Activity-calibrated point sources of ^{65}Zn (301.7 ± 0.37%) Bq and ^{54}Mn (3017.21 ± 0.31 %) Bq were measured in the same geometry used in the procedure described above. From the known activities, gamma-ray emission probabilities and counting time, the experimental efficiencies were determined. The resulting values are shown in Table 4 along with the calculated values from Aramis for energies 835 keV (^{54}Mn) and 1115 keV (^{65}Zn).

Table 4. Peak and total efficiencies obtained with the model described in this work compared to experimental values.

E (keV)	Aramis		Experimental	
	$\varepsilon_P\ 10^{-3}$	$\varepsilon_T\ 10^{-3}$	$\varepsilon_P\ 10^{-3}$	$\varepsilon_T\ 10^{-3}$
834.8	0.898	3.457	0.896 (5)	4.0 (1)
1115.5	0.720	3.273	0.702 (7)	3.7 (1)

It can be seen that the simulated peak efficiencies are in good agreement with the experimental data but the differences between the total efficiencies are meaningful. These differences have been pointed out in many similar works; Utsunomiya et al. [15] state that these differences usually amount to 10% to 20%, and assign them to surface channel effects in HPGe coaxial detectors, therefore not accounted for in our program as well as in most detection efficiency simulation programs. The accuracy of the total efficiency can be investigated experimentally by inducing summing effects in the gamma-ray spectra, which can be done counting a point source like ^{152}Eu or ^{166m}Ho positioned close to the detector. The observed peak areas are related to the gamma-ray emission probabilities by sum-correction factors which depend on the total-to-peak ratio, thus giving information about the effect of the chosen geometry on the total efficiency.

4.3. Comparison with MCNP Code

Table 5 shows some simulated values obtained with MCNP compared to Aramis. The greater differences appear between the total efficiencies, which we relate to the simplified electron transport treatment given in our model, where straggling was not evaluated, and ignoring the photon scattering in the detector capsule. However, the results show that disregarding these effects implied differences smaller than 4 % in this energy range, less significant than the typical difference between experiment and simulation in the total to peak efficiency ratio, as discussed in the previous sub-section.

Table 5. Peak and total efficiencies obtained with the model described in this work compared to those obtained with MCNP code.

E (keV)	Aramis		MCNP	
	$\varepsilon_P\ 10^{-3}$	$\varepsilon_T\ 10^{-3}$	$\varepsilon_P\ 10^{-3}$	$\varepsilon_T\ 10^{-3}$
80.57	2.391	2.550	2.4187 (17)	2.627 (11)
280.46	2.241	3.937	2.2573 (17)	4.1123 (33)
410.94	1.609	3.792	1.6246 (20)	3.9596 (30)
711.68	1.006	3.524	1.0224 (26)	3.6616 (34)
810.28	0.921	3.461	0.9216 (27)	3.5820 (25)
1173.24	0.689	3.231	0.6868 (31)	3.3277 (23)

5. FINAL REMARKS

The effective dimensions determined for the HPGe coaxial detector used in this work are different from those stated in the factory manual, proving once more that simulated efficiencies can only be accepted when experimental data are available to check the results, as have been already pointed out by other authors [7,8].

The developed program is relatively small and fast, making it possible to find the effective detector dimensions, which require many interactions with slightly different model parameters, in short time. Running in a Pentium(R) 4 CPU 3.0 GHz, 512 MB of RAM, Windows XP Professional Version 2002, Service Pack2, the program compiled with Microsoft Visual Studio .NET took less than 2 minutes to calculate the efficiencies for 1332 keV, with 82 million histories.

This work is the first part of a project that will join this code to another C++ code written to calculate summing effect corrections using the nuclear data of the radionuclides and the counting efficiencies, to solve problems related to efficiency calibration and emission probability determination in practical gamma-ray spectrometry experiments where sum effects are important. At this moment, we are using this code to simulate counting efficiencies in geometries such that the summing effect in ^{166m}Ho gamma-ray spectrum is very important.

This code will generate the total and peak efficiency curves to predict the expected and the effective experimental peak areas.

REFERENCES

1. E.D. Cashwell, C. J. Everett, *A practical Manual on the Monte Carlo Method for randon walk problems,* Pergamon, New York & USA (1959).
2. P. R Bevington, K. D. Robinson, *Data reduction and error analysis for the physical sciences*, McGraw-Hill, New York & USA (1992).
3. W. H. Press, S. A. Teukolsky, W. T. Veterling, B. P. Flannery, *Numerical Methods in C*, Cambridge, New York & USA (1992).
4. U. Fano, "Hig-Frequency Limit of Bremsstrahlung in the Sauter Approximation", *Physical Review*, **116**, pp.1156-1158 (1959).
5. L. Kissel, "RTAB: The Rayleigh scattering database. Tables for Elastic Photon-Atom Scattering", http://www-phys.llnl.gov/Research/scattering/elastic.html, (last accessed on May 29, 2007).
6. L. Liye L, M. Jizeng, D. Franck, L. Carlan, Z. Binquan, "Monte Carlo efficiency transfer method for full energy peak efficiency calibration of three type HPGe detectors: A coaxial N-type, a coaxial P-type and four BEGe detectors", *Nuclear Instruments and Methods in Physics Research*, **A 564**, pp. 608-613 (2006).
7. J. C. Hardy, V. E. Iacob, M. Sanchez-Vega, R. T. Enger, P. Lipnik, V. E. Mayes, D. K. Willis, R. G. Helmer, "Precise efficiency calibration of an HPGe detector: source measurements and Monte Carlo calculations with sub-percent precision", *Applyed Radiadion and Isotopes,* **56**, pp. 65-69 (2002).
8. L. Venturini, V. R Vanin, "HPGe detector efficiency calibration for extended sources in the 50-1400 keV energy range", *Applied Radiation and Isotopes*, **44**, pp. 999-1002 (1993).
9. "A General Monte-Carlo N-Particle Transport Code", Los Alamos National Laboratory, reports LA-CP-03-0245/1987 (2003), LA-UR-05-8617 (2005), LA-UR-05-2675 (2005), LA-CP-05-0369 (2005).
10. "LNLNE – LNHB/CEA – Table de Radionucléides", http://eig.unique.ch/nucleaire/donnees-nucleaires/Nuclides/HO-166M_TABLES .PDF (2006).
11. "LNE –LNBH/CEA - Table de Radionucléides", http://eig.unige.ch/nucleaire/donnees-nucleaires/Nuclides/ZN-65_TABLES.PDF (2005).
12. "NBM - LNHB/CEA - Table de Radionucléides", http://eig.unige.ch/nucleaire/donnees-nucleaires/Nuclides/MN-54_TABLES.PDF (2004).
13. "CEA - LNHB/CEA - Table de Radionucléides", http://eig.unige.ch/nucleaire/donnees-nucleaires/Nuclides/CO-60_TABLES.PDF (2006).
14. "BNM – LNHB/CEA - Table de Radionucléides", http://eig.unige.ch/nucleaire/donnees-nucleaires/Nuclides/AM-241_TABLES.PDF (2004).
15. H. Utsonomiya, H. Akimune, K. Osaka, T. Kaihori, K. Furutaka, H. Harada, "Surface chanel effect on γ-ray response functions of coaxial germanium detectors", *Nuclear Instruments and Methods in Physics Research* , **A 548**, pp. 455-463 (2005).